

La³⁺-ZnO Nanostructures: A Synergetic Effect of La³⁺ on Structural, Optical and Dielectric Properties of Zinc Oxide

Anil Kaushik¹, Dr S. K. Chaudhary², Dr Ajay Kumar Mann³

¹Research Scholar, Department of Physics, Baba Mastnath University, Asthal Bohar, Rohtak

²Professor, Department of Physics, Baba Mastnath University, Asthal Bohar, Rohtak

³Associate Professor, Department of Physics, Pt. N. R. S. College, Rohtak

Abstract: The influence of La³⁺ ion substitution on structural, optical, and dielectric properties of ZnO nanostructures synthesized using the co-precipitation process is discussed in this paper. The wurtzite hexagonal structure with space group P63mc is confirmed by the XRD results. The domain size, planner spacing and cell volume of the La/ZnO-400 samples were calculated to be 32.2 nm, 2.6849 nm and 67.018 Å³ respectively. SEM was used to conduct morphological research, element mapping and EDS (scanning electron microscope). The photoluminescence spectra were measured using a photoluminescence spectrometer with a 325 nm excitation wavelength. The stretching of the Zn-O bonds resulted in IR spectra with peaks about 535-640 cm⁻¹, which were detected using an FTIR spectrometer. AC impedance spectroscopy of the La/ZnO-400 sample was performed at 310 K in the frequency range of 5 MHz to 50 Hz. The grain edge resistance of the La/ZnO-300 sample is 36.15 M (at 310 K).

Keywords: La doping, ZnO, SEM, EDS, FT-IR, Photoluminescence, AC Impedance

I. INTRODUCTION

The structural, optical and electrical properties of metal oxide nanoparticles are superior. Due to its large band gap ($E_g=3.2-3.8$ eV) and major applications in solar, catalysis, sensor, actuators and spintronics devices, ZnO has gotten a lot of attention in recent decades [1,2]. Various synthesis methods, such as co-perception, sol-gel, thermal evaporation and hydrothermal were used for the preparation of ZnO or ZnO based nano structures. Among these methods, the co-perception method is primarily used for the synthesis of ZnO (II–VI semiconductor) based nano structures in large enough quantities with low outlay as per desired industrial applications. Because of its multifunctional qualities, ZnO is the single most important metal oxide material. Rocksalt (B1), zinc blende (B3), and wurtzite (B4) are three different crystal formations of ZnO. The hexagonal wurtzite with space group P63mc and lattice constants $a = b = 3.2392$ Å and $c = 5.2132$ Å [3] is the most stable phase in ambient conditions. Zn atoms are tetrahedrally coupled to four oxygen atoms in ZnO nanostructures, and Zn's 3d electrons hybridise with oxygen's 3p electrons [4]. There are numerous more ways to improve the application properties of ZnO nanomaterials, such as altering the size and shape of ZnO nanostructures, or substituting metals or non-metal ions on the A- site of ZnO [5, 6]. Substituting metals or metal oxides have proven to be a successful method for creating unique nanomaterials with tailored physical and chemical properties (such as structural, optical, electrical, and catalytic properties) and a wide range of possible applications [7-8]. Furthermore, nanomaterials containing trivalent rare earth (Ln³⁺) ions substituted on the A-site of ZnO are attracting scientific interest due to their wide range of possible applications in photocatalysis, luminescence, optoelectronics and other fields [8]. We provide a dexterous endeavour in order to imprecisely separate the effect of annealing on structural, morphological, optical and dielectric properties of La³⁺ modified ZnO nanostructures. As a result, in the current study, we used the co-perception technique to synthesis La³⁺ substituted ZnO nanostructures and investigated the effect of annealing temperatures on structural, optical and dielectric properties.

II. EXPERIMENTAL SECTION

1.1. Chemicals & Synthesis Process:

Zinc acetate dehydrate (Zn(CH₃COO)₂), Sodium hydroxide (NaOH), Ethanol (C₂H₅OH), and DI water were used as preliminary materials in this study and did not require further purification. The starting materials or precursors for the conventional co-precipitation synthesis of 'La' modified Zinc Oxide nanoparticles (abridged La/ZnO-RT & La/ZnO-400) were zinc acetate dehydrate and sodium hydroxide in a stoichiometric ratio. These precursors were then dissolved in a mixture of ethanol and DI water. The mixture of these precursors was then agitated for 2 hours at 80 °C. After that,

this solution was left to sit overnight, and then washed multiple times with DI water before being dried in an oven for 12 hours at 90 degrees Celsius. As a result, the resulting powder was annealed at 400°C for 2 hour. Finally, after the full combustion procedure, the white fine powder was obtained.

2.2. Characterizations:

The phase and crystal structure of synthesised La/ZnO-RT and La/ZnO-400 samples were determined using a Rigaku X-ray Diffractometer (wavelength = 1.542 Å), in a scanning angle range 10° to 90° and a scanning step of 2°/min. SEM scans at a 20 kV accelerating voltage were used to investigate the surface morphology, mapping and EDS of La/ZnO-RT and La/ZnO-400 samples. A photoluminescence (PL) spectrometer was used to determine the band gap and emission spectra. The FTIR spectroscopy was used to find the stretching bonds in the samples. Impedance Analyzer was used to conduct impedance tests (SP-240).

III. RESULTS AND DISCUSSIONS

3.1 Structural Analysis:

Figure 1 shows the XRD patterns of synthesized La/ZnO-RT and La/ZnO-400 samples of ‘La’ modified ZnO in the diffraction angle 10° to 90° range. Figure 1 depicts the diffraction peaks at the value of 2θ, 31.73°, 34.28°, 36.27°, 47.59°, 56.34°, 62.55°, 67.96°, 69.11°, 72.47°, 76.99°, and 81.54° correspond to hkl values (100), (002), (101), (102), (110), (103), (200) and (112) respectively. All of the obtained XRD peaks corresponded to JCPDS card #80-0075. Debye Scherer's equation [7] can be used to estimate the mean value of domain size (D):

$$D = 0.9 \lambda / \beta_{hkl} \cos\theta \dots\dots\dots (1)$$

Where, wavelength = 1.54 Å of X-ray, β = is the full width half maximum, θ = is the diffraction angle, and represents the instrumental broadening.

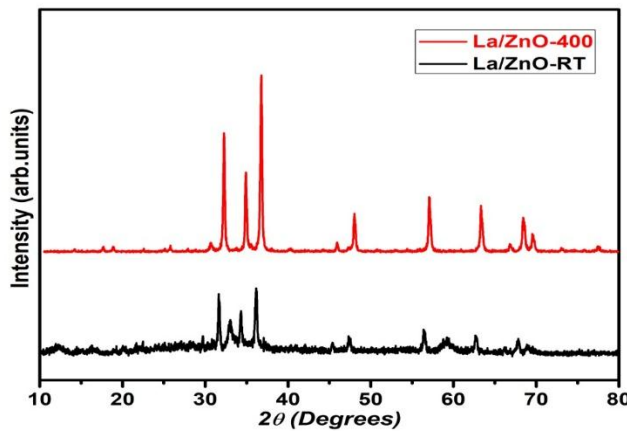


Figure1. XRD patterns of La/ZnO-RT & La/ZnO-400 samples

The sample’s intraplaner (d_{hkl}) was predictable using the Bragg's correlation:

$$2d_{hkl}\sin\theta = n\lambda \dots\dots\dots (2)$$

Where, the diffraction order is ‘n’. The following relationships were used to compute the lattice constants and unit cell volume of the synthesized La/ZnO-RT and La/ZnO-400 samples:

$$a = d_{hkl} * \sqrt{h^2 + k^2 + l^2} \dots\dots\dots (3)$$

$$V = 0.866 * a^2 * c \dots\dots\dots (4)$$

Where d_{hkl} is the intraplaner, hkl is the miller indices of the consequent plane, a & c are the lattice parameters and all of these parameters are summarized in table 1.

Table 1:

Sample Name	Domain size (nm)	d-spacing (d_{hkl}) Å	lattice constants Å		Unit Cell Volume (V) Å ³
			a = b	C	
La/ZnO-400	32.2	2.6849	3.7213	5.6124	67.018

3.2 Morphological Analysis:

Figure 2 (a-b) shows the effect of 'La' on the morphology of $Zn_{0.92}La_{0.08}O$ (La/ZnO-RT & La/ZnO-400) samples using SEM.

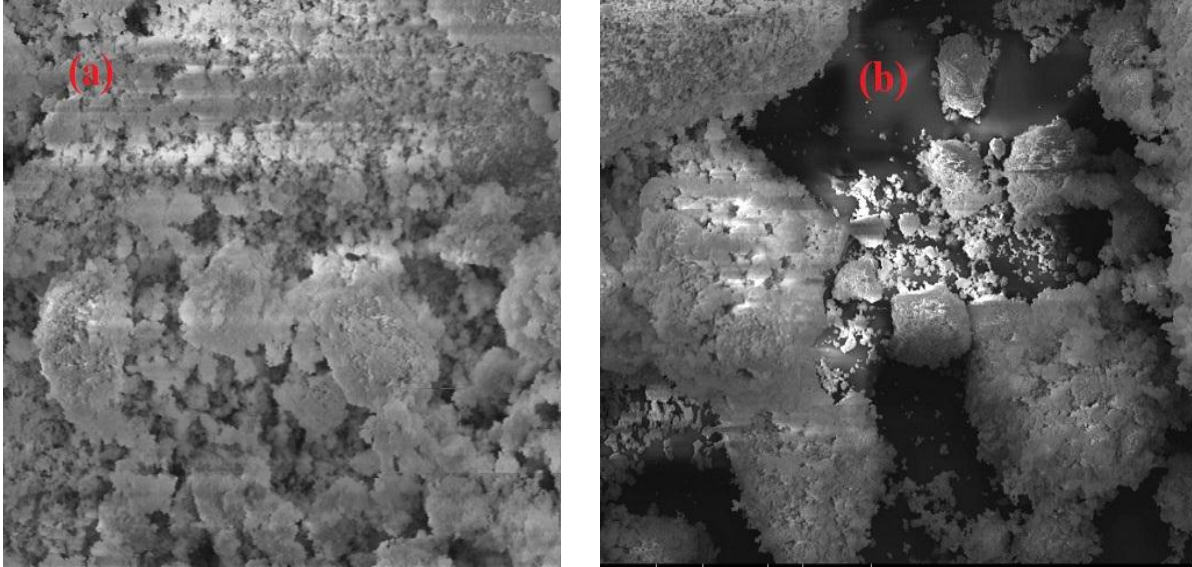


Figure 2: SEM micrographs of (a) La/ZnO-RT & (b) La/ZnO-400 samples.

The micrographs in the figure are polycrystalline and reveal agglomeration, uneven forms and sizes as a result of a high-energy chemical reaction. The uneven distribution of particles in nanostructures may ensure structural, electrical, and many other features. This impact could be caused by their lower diffusivity. With the XRD analysis, these results are likewise reliable.

3.3 PL Analysis:

Figure 3 shows the photoluminescence (PL) spectra of $Zn_{0.92}La_{0.08}O$ (La/ZnO-RT & La/ZnO-400) samples at an excitation wavelength of 380 nm.

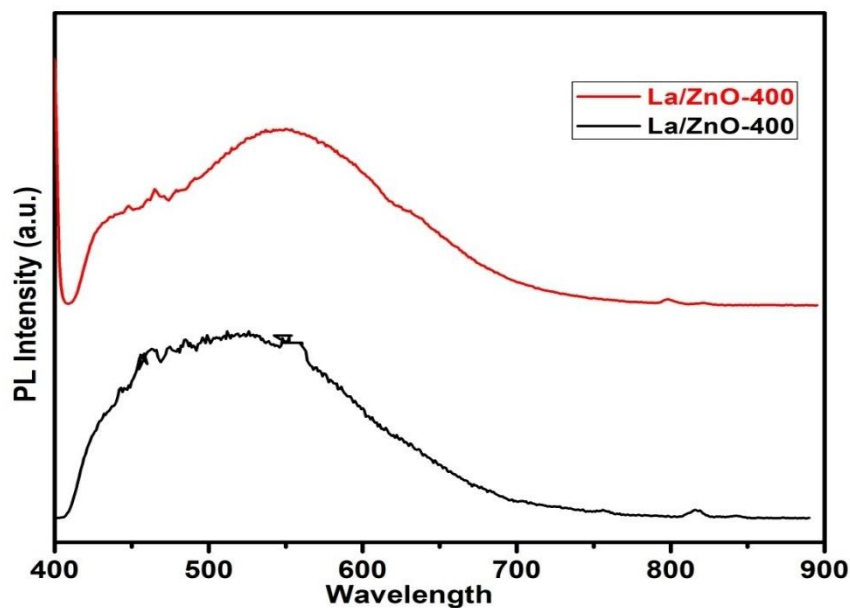


Figure 3: PL spectroscopy of La/ZnO-RT & La/ZnO-400 samples.

There was a strong emission peak centred at 430 and 550 nm, which has a red shift as compared to the near band emission in ZnO. The 'La' ions are created defects in doped ZnO, which may develop minor energy levels close to the conduction band as a result of this. As a result of the created trivial energy levels, the violet emission peak might be

attributed to the recombination centres [8-10]. Furthermore, interstitial Zn ions and oxygen vacancies were created along with the incorporation of 'La', which has a major impact on the optical characteristics of the modified ZnO samples with doping ions.

3.4 FT-IR Analysis:

The FTIR spectra of $Zn_{0.92}La_{0.08}O$ (La/ZnO-RT & La/ZnO-400) samples in the region of wave number 500-3700 cm^{-1} are shown in figure 4.

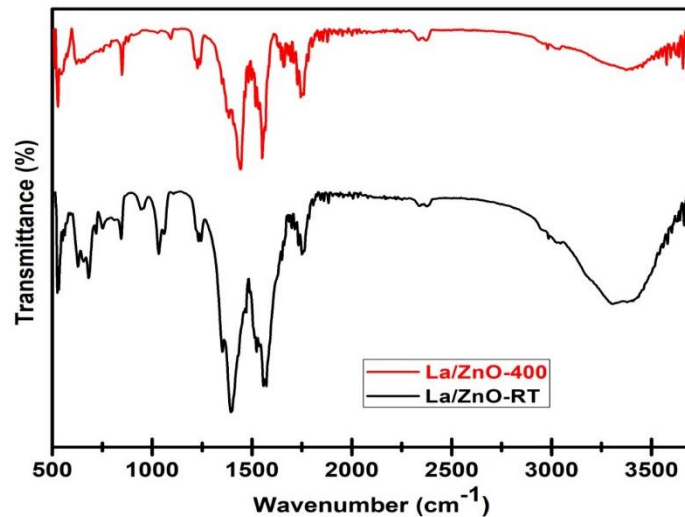


Figure 4: FTIR spectra of La/ZnO-RT & La/ZnO-400 samples.

The IR peaks for the La/ZnO-RT and La/ZnO-400 samples are 3375 cm^{-1} , 2350 cm^{-1} , 1540 cm^{-1} , 1424 cm^{-1} , 1215 cm^{-1} , 825 cm^{-1} , 610 cm^{-1} , and 532 cm^{-1} . The vibration of the C-H, C=O, and C-O bonds is represented by IR peaks ranging from 680 cm^{-1} to 1650 cm^{-1} . The deficient states near to 'La' ions in the Zn-O lattice structure are shown by the small and scruffy absorption bands about 825 cm^{-1} . The stretching of the Zn-O bonds is represented by the peaks between 532-630 cm^{-1} [9, 10]. The remaining peaks, which span from 1700 cm^{-1} to 3300 cm^{-1} , show O-H bond stretching vibrations, bending modes of submerged water, and the presence of O=C=O bonds. The IR peaks sharply appear in the range 500 cm^{-1} to 1500 cm^{-1} as the calcination temperature increases for ZnO sample, which is due to the presence of compressive stress on La/ZnO nanoparticles, increase in crystalline character of La/ZnO, and distinction in morphology of La/ZnO.

3.4 Complex Impedance Spectroscopy (CIS):

Complex impedance measurement is a popular approach for determining the relationship between a sample's electronic transport performance and its structures, as well as providing information on the landscape of electronic states.

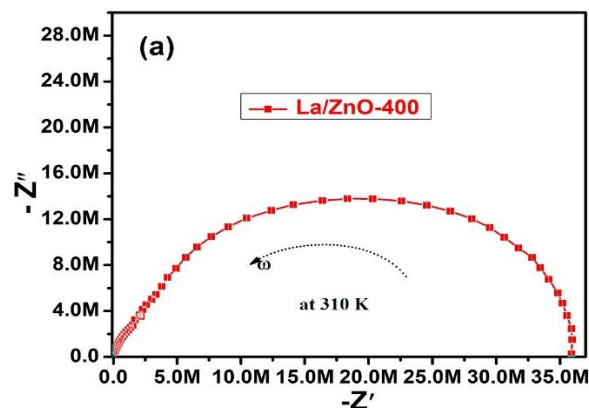


Figure 5 (a): Nyquist (Cole-Cole) plot of La/ZnO-400 samples.

Figure 5 (a) shows the AC impedance ($Z + iZ''$) measurements or Cole-Cole plots of the $Zn_{0.92}La_{0.08}O$ (La/ZnO-400) sample at room temperature in the frequency range 10 Hz to 05 MHz (with applied field 100 mV) (310 K). A relationship gives the complex AC impedance (Z):

$$Z = Z' - jZ'' \dots\dots\dots (5)$$

Where Z' is the real part of complex AC impedance and Z'' is the imaginary part. To eliminate electronic transport driven by visible light in the La/ZnO-400 sample, the impedance spectra are recorded in a dark medium. The complicated impedance curve annexes a separate semicircle curve, which is commonly caused by grain corollary [9-12]. At room temperature, the semicircular curve suggests a massive insulating feature. Furthermore, dielectric relaxation in the low frequency range is linked to domain margin contribution, whereas relaxation at high frequencies is related to domain contribution. Thermally activated charge carriers with larger energy overcome the insulating grain (domain) border and contribute to electronic conduction in semiconducting materials, resulting in this type of activity.

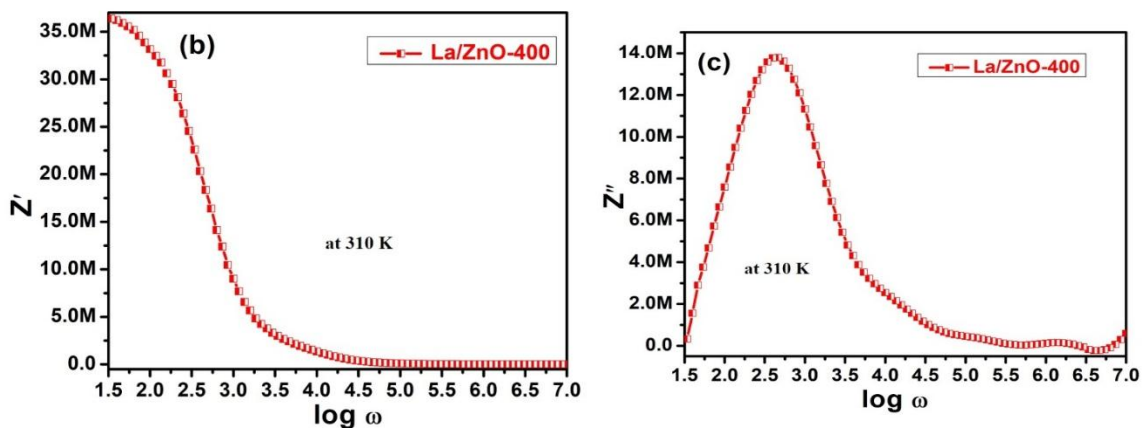


Figure 5 (b).: Variation of real part of Impedance with frequency
(c) Variation of real part of Impedance with frequency for La/ZnO-400 samples.

The semicircles are depicted in Nyquist plots as having two forms of dielectric relaxation phenomena or non Debye type performance [10, 11]. Figure 5 (b) shows the variation of the real fraction (Z') of complex AC impedance as a function of frequency at 310 K, and it is obvious that the values of Z' rapidly fall with frequency, which is related to an increase in AC conductivities due to hopping conduction phenomena [12, 13]. As a result, the real portion of complex impedance has difficult frequency reliant performance in the lower frequency province, which correlates to high resistivity and greater grain boundary resistance values, but Z' demonstrates frequency sovereign behavior in the higher frequency range. Figure 5 (c) depicts the variation of Z'' fraction of impedance as a function of frequency, which shows a behavior that is quite similar to Z' . The grain and grain edge of the crystal structure are ripped using Complex AC Impedance Spectroscopy, which coincides with the lower and higher frequency dispersal zones [12, 14].

IV. CONCLUSION

The Zinc Oxide (ZnO) samples were successfully produced using the co-perception technique at various annealing temperatures in order to investigate the effect of annealing on the synthesis process and characteristics. The ZnO sample calcined at 300 C has crystalline size, inter planner spacing and volume of 36.15 nm, 2.6849 Å, and 67.018 Å³, respectively. The structural, morphological, FTIR and electronic transport properties of both ZnO samples are excellent. The vibration of the C-H, C=O and C-O bonds is represented by the FTIR peaks in the 710 cm⁻¹ to 1730 cm⁻¹ range. The stretching of the Zn-O bonds is represented by the peaks about 535 cm⁻¹. For ZnO calcined at 400°C, the grain boundary resistance is around 36.15 MΩ (at 310 K). In the low frequency range, the real part of complex impedance has a strong frequency dependent behaviour, which translates to increased resistivity and high grain boundary resistance values.

Aknowledgement:

The authors are grateful for the facilities provided by the Department of Physics at Baba Mastnath University, Asthal Bohar, Rohtak.

REFERENCES

- [1]. D. Gao, et al., Room temperature ferromagnetism of pure ZnO nanoparticles, *Journal of applied physics* 105.11 (2009): 113928.
- [2]. B. Sharma et al., Synthesis and characterization of polyaniline–ZnO composite and its dielectric behavior, *Synthetic metals* 159.5-6 (2009): 391-395.
- [3]. T. Sahoo et al., Synthesis and characterization of porous ZnO nanoparticles by hydrothermal treatment of as pure aqueous precursor, *Materials Research Bulletin* 46.4 (2011): 525-530.
- [4]. S. B. Rana, et al., Synthesis and characterization of pure and doped ZnO nanoparticles, *Journal of Optoelectronics and Advanced Materials* 12.2 (2010): 257.
- [5]. [S. Muthukumaran and R. Gopalakrishnan, Structural, FTIR and photoluminescence studies of Cu doped ZnO nanopowders by co-precipitation method, *Optical Materials* 34.11 (2012): 1946-1953.
- [6]. Jakeer Husain; Rehana Anjum; Shivaraj G; Gavisiddhaya Mathad; Deepa Pathar; Jaisheel Sagar; Bushara Anjum. "Electrical properties of polyaniline/Cadmium Oxide/ZnO Nanocomposites Thin Films". *International Research Journal on Advanced Science Hub*, 2, 8, 2020, 31-33. doi: 10.47392/irjash.2020.89
- [7]. K. Raja et al., Structural, FTIR and photoluminescence studies of Fe doped ZnO nanopowder by co-precipitation method, *Spectrochimica acta part A: molecular and biomolecular spectroscopy* 131 (2014): 183-188.
- [8]. Rashmi S.K; H.S. Bhojya Naik; Jayadevappa H. "Optical and photocatalytic application of ZnFe₂O₄–SmFeO₃ nanocomposites". *International Research Journal on Advanced Science Hub*, 2, 8, 2020, 123-130. doi: 10.47392/irjash.2020.105
- [9]. Jakeer Husain; Rehana Anjum; Narsappa Reddy; Jaisheel Sagar; Bushara Anjum. "AC Conductivity Studies on Polyaniline/Cobalt Oxide Nanocomposites Thin Films". *International Research Journal on Advanced Science Hub*, 2, 7, 2020, 41-43. doi: 10.47392/irjash.2020.62
- [10]. S. P. Singh et al., EPR, FTIR, optical absorption and photoluminescence studies of Fe₂O₃ and CeO₂ doped ZnO–Bi₂O₃–B₂O₃ glasses, *Journal of alloys and compounds* 493.1-2 (2010): 256-262.
- [11]. M. Sajjad et al., Structural and optical properties of pure and copper doped zinc oxide nanoparticles, *Results in Physics* 9 (2018): 1301-1309.
- [12]. R. Zamiri et al., Structural and dielectric properties of Al-doped ZnO nanostructures, *Ceramics International* 40.4 (2014): 6031-6036.
- [13]. Tabib et al., Investigations on electrical conductivity and dielectric properties of Na doped ZnO synthesized from sol gel method, *Journal of alloys and compounds* 622 (2015): 687-694.
- [14]. M. Okutan et al., AC conductivity and dielectric properties of Co-doped TiO₂, *Physica B: Condensed Matter* 364.1-4 (2005): 300-305.
- [15]. T. Nachaithong et al., Preparation, characterization, and giant dielectric permittivity of (Y³⁺ and Nb⁵⁺) co-doped TiO₂ ceramics, *Journal of the European Ceramic Society* 37.11 (2017): 3521-3526.
- [16]. D. A. Crandles et al., Electrode effects in dielectric spectroscopy measurements on (Nb⁺ In) co-doped TiO₂, *Journal of Applied Physics* 119.15 (2016): 154105.
- [17]. J. A. Mergos and C. T. Dervos, Structural and dielectric properties of Li₂O-doped TiO₂, *Materials characterization* 60.8 (2009): 848-857.